

# INLA or MCMC? A Tutorial and Comparative Evaluation for Spatial Prediction in log-Gaussian Cox Processes

Benjamin M Taylor and Peter J Diggle

November 27, 2024

## Abstract

We investigate two options for performing Bayesian inference on spatial log-Gaussian Cox processes assuming a spatially continuous latent field: Markov chain Monte Carlo (MCMC) and the integrated nested Laplace approximation (INLA). We first describe the device of approximating a spatially continuous Gaussian field by a Gaussian Markov random field on a discrete lattice, and present a simulation study showing that, with careful choice of parameter values, small neighbourhood sizes can give excellent approximations. We then introduce the spatial log-Gaussian Cox process and describe MCMC and INLA methods for spatial prediction within this model class. We report the results of a simulation study in which we compare MALA and the technique of approximating the continuous latent field by a discrete one, followed by approximate Bayesian inference via INLA over a selection of 18 simulated scenarios. The results question the notion that the latter technique is both significantly faster and more robust than MCMC in this setting; 100,000 iterations of the MALA algorithm running in 20 minutes on a desktop PC delivered greater predictive accuracy than the default INLA strategy, which ran in 4 minutes and gave comparative performance to the full Laplace approximation which ran in 39 minutes.

# 1 Introduction

The primary aim of this article is to provide an objective comparison of two methods for Bayesian Inference in the spatial log-Gaussian Cox process: a relatively slow but asymptotically exact method, Markov chain Monte Carlo (MCMC); and a faster but approximate method, the integrated nested Laplace approximation (INLA). The secondary aim is to provide a tutorial in some of the technical aspects involved with computation and inference for this class of models.

The log-Gaussian Cox process is but one of a number of possible model classes that we could have used as the basis for a comparative evaluation of MCMC and INLA methods. Our specific motivation for focusing on this model is its use in spatial epidemiology, and specifically in health surveillance applications, where interest is in the predictive probability that the relative risk of disease at a certain spatial location exceeds a threshold set by public health experts. For an example in the spatio-temporal setting see Diggle et al. (2005). There, the data consisted of locations of incident cases each day, i.e. a spatio-temporal point process, and the Cox process was used to represent spatio-temporal variation in risk as a product of deterministic and stochastic terms representing, respectively, known risk-factors and unexplained variation, prediction of which was the primary goal. A high predictive probability that risk in a particular area exceeds the pre-declared threshold may activate a costly public health intervention, hence it is important that such predictive probability statements are as accurate as possible. For this reason we will compare MCMC and INLA using a metric that directly measures their ability to make accurate predictive probability statements.

MCMC methods have made an enormous impact on statistical practice by making Bayesian inference tractable for complex statistical models, including models whose specification includes a latent Gaussian process. However, they can be computationally burdensome and, more importantly, their inferential validity rests on the convergence of a Markov chain to its

equilibrium distribution, which can be difficult to verify empirically. INLA (Rue et al., 2009) is a recently developed competitor to MCMC methods. By using a combination of analytical approximation and numerical integration rather than Monte Carlo simulation, INLA circumvents the convergence issues that arise with MCMC methods, and typically leads to quicker computation. However, the price paid is that the analytic approximations potentially introduce errors in the calculation of posterior probabilities. The goal of the simulation study in this paper is to assess the trade-off between faster computation and errors of approximation.

Our focus is on predicting (functions of) a latent spatially continuous Gaussian process  $\mathcal{Y}$ , which we approximate by a Gaussian field,  $Y$ , on a finely spaced, regular square grid of points on the plane. This is in contrast to the methods discussed in Lindgren et al. (2011), in which a representation is constructed on a triangulation of a set of irregularly spaced points. Lindgren et al. (2011) assume that  $\mathcal{Y}$  has Matérn second order structure, that is for  $u, v \in \mathbb{R}^2$ ,

$$\text{cov}(u, v) = \frac{\sigma^2}{\Gamma(\nu)2^{\nu-1}} (\kappa \|v - u\|)^\nu K_\nu(\kappa \|v - u\|),$$

where  $\nu, \kappa > 0$  and  $K_\nu$  is a modified Bessel function of the second kind. The major advantage of their approach is its low computational cost: for any choice of the admissible parameters of the covariance function, they are able to compute the precision matrix of the GMRF approximation in  $O(n)$  time, where  $n$  is the number of triangulation points. We prefer to retain greater flexibility in choosing an appropriate model for the covariance, allowing data and scientific knowledge to inform this choice. For this reason, we focus instead on the method described in Chapter 5 of Rue and Held (2005), which allows effectively any covariance model to be fitted to the data.

In Section 2, we discuss the approximation of a spatially continuous Gaussian process by a Gaussian Markov random field, and give the results of a simulation study detailing the effectiveness of this procedure. In Section 3, we describe the spatial log-Gaussian Cox process. Sections 4 and 5 give details of the MCMC and INLA methods, respectively. Section 6

summarises the findings. Section 7 is a concluding discussion. Throughout the article, we use  $\pi$  to denote a generic probability density function.

All of the methods discussed in the article are implemented in the R package `lgcp`; see Taylor et al. (2011).

## 2 Spatially Continuous Gaussian processes and their Approximation by Gaussian Markov Random Fields

In this section, we consider how to approximate a spatially continuous Gaussian process by a GMRF and, via simulation, how good such an approximation is. Note that a discussion of this topic is given in Chapter 5 of Rue and Held (2005). To begin, we introduce some more general concepts.

### 2.1 Theory

A spatially continuous Gaussian process,  $\mathcal{Y}$ , is a real-valued continuous Gaussian process on the plane,  $\mathbb{R}^2$ . This means that  $\mathcal{Y}$  is a continuous function from  $\mathbb{R}^2 \rightarrow \mathbb{R}$  with the property that for any finite collection of locations,  $\{s_i\}_{i=1}^n$ , the joint distribution of the random variables representing the value of the process at each of the locations,  $\{\mathcal{Y}(s_i)\}$ , is multivariate Gaussian.  $\mathcal{Y}$  is called *strictly stationary* if  $\mathbb{E}(\mathcal{Y}(s_i)) = \alpha$  for some  $\alpha \in \mathbb{R}$  and any spatial location  $s_i$  and *strictly second-order stationary and isotropic*, if the covariance between  $\mathcal{Y}(s_i)$  and  $\mathcal{Y}(s_j)$  only depends on the Euclidean distance between  $s_i$  and  $s_j$ , denoted by  $\|s_i - s_j\|$  (Gelfand et al., 2010). The covariance between  $u, v \in \mathbb{R}^2$  will be assumed to have the form,

$$\text{cov}(u, v) = \sigma^2 r(\|v - u\|/\phi),$$

where  $r$  is a standard isotropic correlation function: for example a Matérn function. The parameter  $\sigma$  dictates the point-wise variability of the field, whilst the scale parameter  $\phi$  governs the rate of decay of the correlation in space. In what follows, an italic Roman,  $Y$ , will be used to denote the values of  $\mathcal{Y}$  at a finite set of locations in space. We say that  $Y$  *represents* the process  $\mathcal{Y}$ .

A Gaussian Markov random field is a collection of random variables,  $\tilde{Y} = \{\tilde{Y}_1, \dots, \tilde{Y}_k\}$ , that have a multivariate Gaussian distribution,  $\tilde{Y} \sim \text{MVN}(\tilde{\mu}, \tilde{Q}^{-1})$ , where for any  $j$ ,

$$[\tilde{Y}_j | \tilde{Y}_{-j}] = [\tilde{Y}_j | \text{the neighbours of } \tilde{Y}_j],$$

where  $\tilde{Y}_{-j}$  denotes  $\{\tilde{Y}_1, \dots, \tilde{Y}_{j-1}, \tilde{Y}_{j+1}, \dots, \tilde{Y}_k\}$  and  $[\cdot]$  means ‘the distribution of’. We use  $Y$   $\tilde{Y}$  to distinguish between respectively the Gaussian field and the Gaussian Markov random field representation of a process  $\mathcal{Y}$  at the same finite set of locations. The *neighbours* of  $j$ ,  $\mathcal{N}_j$ , are usually a much smaller subset of  $\tilde{Y}$ ; all other elements of  $\tilde{Y}$  are conditionally independent of  $\tilde{Y}_j$ , given  $\mathcal{N}_j$ . The pattern of conditional independence is evident in the precision matrix,  $\tilde{Q}$ : Theorem 2.2 in Rue and Held (2005) states that,

$$\tilde{Y}_i \perp\!\!\!\perp \tilde{Y}_j | \mathcal{N}_i \cup \mathcal{N}_j \iff \tilde{Q}_{ij} = 0.$$

In the case that the neighbourhoods of each element are very small subsets of  $\tilde{Y}$ , the matrix  $\tilde{Q}$  is sparse. This allows otherwise computationally prohibitive operations, such as matrix inversion, to be implemented with fast algorithms.

To simplify matters, consider a square observation window,  $W$ , on which a spatially continuous Gaussian process is represented by a finite collection of random variables  $Y = \{Y_{ij}\}_{i,j=1}^M$  spaced on a regular square grid,  $G = \{G_{ij}\}_{i,j=1}^M$ , where the  $G_{ij}$  are the centroids of grid cells, that cover  $W$ . For computational reasons to be explained, we assume that  $M = 2^m$  for some positive integer  $m$ . In order to obtain a representation of the *stationary* second order structure of the process, it is necessary to extend this grid, typically to a grid of size

$2M \times 2M$ , which is wrapped on a torus. This action gives rise to the notion of a toroidal distance metric, by which is meant the minimum distance between two points, travelling either directly (e.g. if the points were very close together on the torus) or around the minor and/or major radii. A precise definition is given in Møller et al. (1998).

Let  $Y^{\text{ext}} = \{Y_{ij}^{\text{ext}}\}_{i,j=1}^{2M}$  be random variables at grid locations  $G^{\text{ext}} = \{G_{ij}^{\text{ext}}\}_{i,j=1}^{2M}$  on the extended space. Note that in cases where the spatial decay parameter,  $\phi$ , is quite quite large compared with the size of  $W$ , then in order to obtain a valid covariance structure, the grid may have to be extended further, e.g. onto a  $4M \times 4M$  toroidal grid, see for example Møller et al. (1998). The covariance matrix,  $\Sigma_{\text{ext}}$ , of the discrete field  $Y^{\text{ext}}$  on the extended grid is typically massive, dense and with a dense inverse,  $Q_{\text{ext}}$ . As an example, for a  $128 \times 128$  grid in the extended space, the covariance matrix has dimension  $16384 \times 16384$ : the storage and manipulation of such matrices under ordinary circumstances is not computationally feasible on a desktop PC. However, in the extended space,  $\Sigma_{\text{ext}}$  is block-circulant (see below) and symmetric positive definite (SPD) with a block circulant SPD inverse,  $Q_{\text{ext}}$ . The symmetry induced in the covariance matrix by extending the grid and wrapping it on a torus means that each entry of  $\Sigma_{\text{ext}}$  is one of exactly  $(2M)^2 = 128^2 = 16,384$  elements, instead of a possible  $16,384^2 = 268,435,456$  different elements. Furthermore, matrix computation in the extended space is greatly aided by using the discrete Fourier transform (DFT), which is why the focus of this article is on grids of dimension  $2^m \times 2^m$ . In fact, it is possible to drop this assumption, at the price of reduced speed in the DFT. Algorithms are available to construct optimised computational plans for implementing the DFT on other grid sizes, for example the FFTW library (Frigo and Johnson, 2011) and an R wrapper library (Krey et al., 2011). In what follows, DFT and IDFT will denote, respectively, the discrete Fourier and discrete inverse-Fourier Transforms; as an abuse of notation, the same abbreviations will be used for the 1- and 2-dimensional transforms, with the choice being context dependent (Wood and Chan, 1994).

A full discussion of why and how the DFT is used in matrix computations on block circulant

matrices is given in Chapter 2 of Rue and Held (2005), but for completeness a very brief summary follows. An  $n \times n$  matrix  $A$  is said to be *circulant* if it has the following structure:

$$A = \begin{bmatrix} a_0 & a_1 & \cdots & a_{n-1} \\ a_{n-1} & a_0 & \cdots & a_{n-2} \\ \vdots & \vdots & & \vdots \\ a_1 & a_2 & \cdots & a_0 \end{bmatrix},$$

where  $a_i$  belong to a field, for example the real numbers. The ordered set of elements,  $\tilde{a} = \{a_j\}_{j=1}^n$ , is called the base of  $A$ . A real  $nm \times nm$  block circulant matrix  $C$  is one with the following structure:

$$C = \begin{bmatrix} A_0 & A_1 & \cdots & A_{m-1} \\ A_{m-1} & A_0 & \cdots & A_{m-2} \\ \vdots & \vdots & & \vdots \\ A_1 & A_2 & \cdots & A_0 \end{bmatrix},$$

where each  $A_i$  is a circulant matrix with base  $\tilde{a}_i = \{a_{ij}\}_{j=0}^{n-1}$ . The matrix

$$\tilde{c} = \begin{bmatrix} a_{00} & a_{10} & \cdots & a_{(m-1)0} \\ a_{01} & a_{11} & \cdots & a_{(m-1)1} \\ \vdots & \vdots & & \vdots \\ a_{0(n-1)} & a_{1(n-1)} & \cdots & a_{(m-1)(n-1)} \end{bmatrix}$$

is known as the base matrix of  $C$ .

The eigenvectors of a circulant matrix  $A$  (as defined above) can be written as

$$E_j = \sum_{i=0}^{n-1} a_i \exp\{-2\pi i j / n\}.$$

The complete set of eigenvectors are stored in columns of the (unitary) discrete Fourier

transform matrix,

$$F = \begin{bmatrix} 1 & 1 & 1 & \dots & 1 \\ 1 & \omega & \omega^2 & \dots & \omega^{n-1} \\ 1 & \omega^2 & \omega^4 & \dots & \omega^{2(n-1)} \\ \vdots & \vdots & \vdots & \ddots & \vdots \\ 1 & \omega^{n-1} & \omega^{2(n-1)} & \dots & \omega^{(n-1)(n-1)} \end{bmatrix},$$

where  $\omega = \exp\{2\pi i/n\}$ . Now, let  $E$  be a diagonal matrix with the eigenvalues  $\{E_j\}_{j=0}^{n-1}$  on the leading diagonal. By expanding the matrix product analytically it is straightforward to verify that the matrix  $A$  has spectral decomposition,  $A = FEF^H$ , where the superscript  $H$  denotes the conjugate transpose. The most useful aspect of the matrix  $F$  is that matrix-vector products  $Fv$  and  $F^Hv$  are available directly as the DFT and IDFT, respectively, of the vector  $v$ . The vector  $E$  is available as  $E = \sqrt{n}F\tilde{a}$  and matrix square roots are computed from expressions such as  $A^{1/2} = FE^{1/2}F^H$ . These results massively simplify computation with ordinary circulant matrices; furthermore, the theory extends to block circulant matrices, where the 2-dimensional DFT and IDFT are used.

In what is to follow the ‘full covariance matrix’ will mean the covariance matrix of  $Y^{\text{ext}}$ , i.e.  $\Sigma_{\text{ext}}$ . For the application in mind, namely the spatial log-Gaussian Cox process, it has been argued that Markov chain Monte Carlo using the full covariance matrix is inefficient (Rue et al., 2009; Simpson et al., 2011). The suggested alternative is to use the integrated nested Laplace approximation to perform approximate Bayesian inference with a sparse GMRF approximation to the full covariance matrix so as to reduce computational cost. We now discuss the construction of such a GMRF approximation.

For the full covariance matrix defined by an arbitrary choice of correlation function, the dependence structure is ‘dense’: there is no sparse conditional independence structure – the precision matrix  $Q_{\text{ext}}$  is a dense matrix. A GMRF approximation to  $\Sigma_{\text{ext}}$  is constructed by parametrising the precision matrix,  $\tilde{Q}_{\text{ext}} \equiv \tilde{Q}_{\text{ext}}(\theta)$ , and choosing  $\theta_{\text{opt}}$  to be such that  $\tilde{Q}_{\text{ext}}(\theta_{\text{opt}})^{-1} = \tilde{\Sigma}_{\text{ext}}(\theta_{\text{opt}})$  is ‘as close as possible’ to  $\Sigma_{\text{ext}}$ . The parametrisation considered here



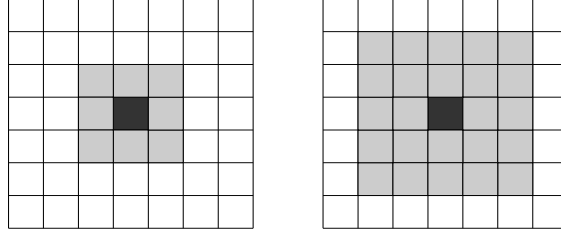


Figure 1: Illustrating the choice of 1- and 2-neighbourhoods, respectively the left and right hand plots. The black square is the grid cell of interest and the grey cells are those specified to be the neighbours in the chosen level of dependence.

is similar to that presented in Chapter 5 of Rue and Held (2005), in which the neighbourhood of a grid cell consists of all the cells in the box surrounding the cell of interest, up to a certain distance away. Figure 1 illustrates what will be referred to in this article as 1- and 2-neighbourhoods: the box obtained by specifying respectively dependence on all cells in the box a distance of up to 1 and up to 2 cells both vertically and horizontally around the cell of interest. For the 1-neighbourhoods,  $\theta$  has 3 elements, corresponding to the dependences between cells a distance 0 apart, between directly adjacent cells and between diagonally adjacent cells. In a similar way, for the 2-neighbourhood dependence structure,  $\theta$  has six elements.

Let  $\varsigma$  be the base matrix of  $\Sigma_{\text{ext}}$  and let  $\hat{\varsigma}(\theta)$  be the base of the inverse of  $\tilde{Q}_{\text{ext}}$ , with base matrix  $\tilde{\psi}(\theta)$ . Note that,  $\hat{\varsigma}(\theta)$  can be computed from  $\tilde{\psi}(\theta)$  using the 2-dimensional discrete Fourier transform,

$$\hat{\varsigma}(\theta) = \frac{1}{\text{length}\{\text{vec}[\tilde{\psi}(\theta)]\}} \text{IDFT}(\text{DFT}(\tilde{\psi}(\theta)) \otimes (-1)),$$

where  $X \otimes (-1)$  denotes the raising of each element of matrix  $X$  to the power  $-1$  and  $\text{vec}(X)$  is the vector obtained by stacking the columns of  $X$  on top of each other. The optimal  $\theta$  is

found as  $\min_{\theta} \{U(\theta)\}$  where,

$$U(\theta) = \sum_{ij} w_{ij} (\varsigma_{ij} - \hat{\varsigma}(\theta)_{ij})^2,$$

where a subscript  $ij$  denotes the  $(i, j)$ -element of the matrix,

$$w_{ij} \propto \begin{cases} 1 & \text{if } ij = (0, 0) \\ \frac{1+a/d(i,j)}{d(i,j)} & \text{otherwise} \end{cases}$$

Here,  $d(i, j)$  is the distance from cell  $(i, j)$  to the reference origin  $(0, 0)$  and  $a$  is a constant, set equal to 1 in the experiments below, see Rue and Held (2005) for a justification of this choice.

Differentiating  $U$  with respect to the  $k$ th component of the parameter,  $\theta_k$ , gives

$$\frac{\partial U(\theta)}{\partial \theta_k} = -2 \sum_{ij} w_{ij} (\varsigma_{ij} - \hat{\varsigma}(\theta)_{ij}) \frac{\partial \hat{\varsigma}(\theta)_{ij}}{\partial \theta_k},$$

which can also be computed using the DFT, since

$$\frac{\partial \varsigma(\theta)}{\partial \theta_k} = \frac{1}{\text{length}\{\text{vec}[\tilde{\psi}(\theta)]\}} \text{IDFT} \left\{ -[\text{DFT}(\tilde{\psi}(\theta)) \oslash (-2)] \odot \text{DFT} \left[ \frac{\partial}{\partial \theta_k} \tilde{\psi}(\theta) \right] \right\}.$$

where  $\odot$  denotes element-wise multiplication, and the matrix  $\frac{\partial}{\partial \theta_k} \tilde{\psi}(\theta)$  is a matrix of 1's where  $\theta_k$  appears and 0's otherwise.

With the above ingredients, standard software such as the `optim` function in R can be used to compute optimal parameters. In particular, the availability of the gradient function enables the user to take advantage of gradient-based optimisation methods such as the `BFGS` method implemented in `optim`. A sensible starting point for the optimiser is given by the base matrix of the diagonal precision matrix,  $\text{diag}(1/\sigma^2)$ .

The reader who is daunted by the prospect of implementing the above functions should note

that this has already been done in the `lgcp` R package (Taylor et al., 2011).

## 2.2 Simulation Study

We performed a simulation study to investigate the ability of the algorithm detailed above to approximate a spatially continuous Gaussian process, and hence choose an appropriate neighbourhood size for use later in the article (see Section 6).

Given a set of parameters of the latent field, an observation window and a grid size, it is possible to compute the base matrix of  $\Sigma_{\text{ext}}$ . With the same inputs and an optimisation step, it is also possible to compute the base matrix of the sparse representation,  $\tilde{\Sigma}_{\text{ext}}(\theta_{\text{opt}})$ . A measure of the performance of the approximation is given by the mean square error in simulating Gaussian random variables. Given a vector of standard Gaussian variates,  $\Gamma$ , a realisation of a Gaussian field with mean  $\mu$  and the correct second order properties is given by  $y = \mu + \Sigma_{\text{ext}}^{1/2}\Gamma$ , whilst an approximation of the field is  $\tilde{y} = \mu + \tilde{\Sigma}_{\text{ext}}^{1/2}\Gamma$ . To compare how well the field has been approximated, an appropriate measure is the integrated mean square error. We estimate this from a repeated sequence of  $n$  independent realisations of  $\Gamma$  as

$$\text{MSE} = \frac{1}{nM^2} \sum_{i=1}^n \sum_{j=1}^M \sum_{k=1}^M (y_{ijk} - \tilde{y}_{ijk})^2, \quad (1)$$

where  $y_{ijk}$  is the value of the  $(j, k)$  cell of  $y$  for the  $i$ th realisation of  $\Gamma$  and  $M$  is the number of grid cells in each direction (here, the grid is assumed to be square). Figure 2 is a visualisation of a true field and two possible sparse approximations using 1- and 2-neighbourhoods.

For the simulation study, the value of  $\sigma$  was fixed at 1 and  $\phi$  allowed to vary between 0.025 and 0.2 with the unit square as the observation window. The parameter  $\sigma$  was fixed because the computed mean square errors would simply scale linearly with  $\sigma^2$ . The range of values of  $\phi$  was chosen to include a selection of scenarios that might be encountered in practice; the important factor is the size of  $\phi$  with respect to the observation window and the grid. When

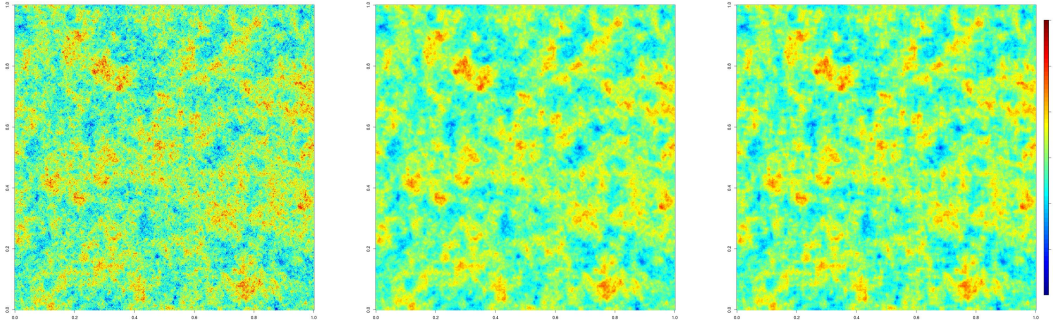


Figure 2: Simulated Gaussian fields. Middle plot: the true field with full covariance structure; left-hand plot: approximate field with a 1-neighbourhood; right-hand plot: approximate field with a 2-neighbourhood. The simulation took place on a  $512 \times 512$  grid, the optimisation took respectively 64 and 355 seconds to compute the parameters of the 1- and 2- neighbourhoods. The result from the 2-neighbourhood is virtually indistinguishable to the eye from the true field, whereas the 1-neighbourhood has a grainy appearance. The respective MSE's were 0.38 and 0.007.

$\phi$  is small compared to the size of the grid, the cells become approximately independent. It should be harder to obtain a good approximation to the latent field for larger values of  $\phi$ , as in this case spatial dependence can be significant for cells a moderate distance apart on the grid. To reduce the possibility of results depending on an artefact of the choice of grid size, two different resolutions were used:  $128 \times 128$  and  $256 \times 256$  in the extended space. For the comparison of  $x$  and  $\tilde{x}$ , the parameter  $\mu$  was set to zero.

Table 1 presents the results of the simulation study. There was a significant improvement in the approximation using a neighbourhood size of 2 compared with a neighbourhood size of 1. The 3-neighbourhood approximations did not appear to improve the quality of the estimated latent field, but were more robust: for the 2-neighbourhood results, the `BFGS` option within `optim` appeared to converge to a local sub-optimal value on two of the occasions, but improved results were obtained by the `Nelder-Mead` simplex option in these cases.

The main conclusions from this study are as follows: (1) it is possible to compute a very good sparse approximation to a given Gaussian field for sensible values of  $\phi$  compared with the size of the observation window; (2) the optimisation time is quick: around a minute for  $256 \times 256$  grids; (3) the optimisation step is not always robust, so in practice, building in a simulation

Ext. Grid	$\phi$	MSE 1	MSE 2	MSE 3	Bias 1	Bias 2	Bias 3
128	0.025	0.086 (0.6)	0.014 (6.2)	0.023 (9.7)	$1.179 \times 10^{-4}$	$3.86 \times 10^{-5}$	$1.424 \times 10^{-5}$
128	0.05	0.174 (1.1)	0.025 (6.4)	0.062 (9.8)	$5 \times 10^{-4}$	$1.333 \times 10^{-4}$	$0.618 \times 10^{-4}$
128	0.1	0.283 (1.1)	0.016 (6.5)	0.042 (9.8)	0.002	$4.332 \times 10^{-4}$	$1.891 \times 10^{-4}$
128	0.15	0.358 (1)	0.018 (6.7)	0.03 (9.8)	0.003	0.001	$4.338 \times 10^{-4}$
128	0.2	0.419 (1.5)	0.031 (6.8)	0.064 (9.9)	0.004	0.001	0.001
256	0.025	0.173 (5.2)	0.024 (33.6)	0.005 (58.5)	$-1.92 \times 10^{-4}$	$-0.535 \times 10^{-4}$	$-1.005 \times 10^{-5}$
256	0.05	0.278 (5.6)	0.024 (35.4)	0.034 (59.7)	-0.001	$-1.848 \times 10^{-4}$	$-0.703 \times 10^{-4}$
256	0.1	0.389 (7.7)	0.041 (35.4)	0.069 (61.5)	-0.002	-0.001	$-3.078 \times 10^{-4}$
256	0.15	0.462 (6.6)	1.677* (32.7)	0.051 (61)	-0.004	-0.003	-0.001
256	0.2	0.515 (8.5)	1.826** (27.1)	0.051 (58.6)	-0.004	-0.003	-0.001

Table 1: Table illustrating the ability of a GMRF to approximate a GF on a unit square observation window. ‘Ext. Grid’ is the size of the DFT grid used, giving respective output grid sizes of  $64 \times 64$  and  $128 \times 128$ ; ‘MSE 1–3’ denotes the mean square error for respective neighbourhood sizes 1–3, with computation time in seconds in parenthesis; and ‘Bias 1–3’ is the mean bias. Optimisation was performed using the ‘BFGS’ method in R’s `optim` command. Using the Nelder-Mead simplex method, the two exceptional values, marked \* and \*\* had improved MSE’s of 0.284 and 0.378. On these occasions, it appeared that the BFGS optimiser had converged to a sub-optimal set of parameters.

step such as described above, i.e. computing  $x$  and  $\tilde{x}$  for a range of  $\Gamma$ , is worthwhile in order to evaluate the approximation; finally (4) for the purposes of the simulation study in Section 6, the 2-neighbourhoods should be sufficiently accurate, because the values of  $\phi$  considered in Section 6 are sufficiently small compared with the observation window.

### 3 The Spatial Log-Gaussian Cox Process

Let  $W \subset \mathbb{R}^2$  be an observation window in space. Events occur at spatial positions  $s \in W$  according to an inhomogeneous spatial Cox process with intensity function  $R(s)$ . Conditional on  $R$ , the number of events,  $X_S$ , occurring in any  $S \subseteq W$  is Poisson distributed (Møller et al., 1998),

$$X_S \sim \text{Poisson} \left\{ \int_S R(s) ds \right\}. \quad (2)$$

Following Diggle et al. (2005), we decompose the intensity multiplicatively as,

$$R(s) = \mu\lambda(s) \exp\{\mathcal{Y}(s)\}. \quad (3)$$

In Equation 3, the *fixed spatial component*,  $\lambda : \mathbb{R}^2 \mapsto \mathbb{R}_{\geq 0}$ , is a known function, proportional to the average intensity of the process at each point in space and scaled so that

$$\int_W \lambda(s) ds = 1, \quad (4)$$

whilst  $\mu$  is the expected number of events in  $W$ . The function  $\mathcal{Y}$  captures the residual variation and is a continuous spatial Gaussian process. The components  $\lambda$  and  $\mu$  define the expected behaviour of the point process, whereas  $\mathcal{Y}$  determines the residual variation. When  $\lambda$  and  $\mu$  are known, it is this residual variation that is of statistical interest: inference about  $\mathcal{Y}$  gives information on extraneous spatial clustering of events, with many applications in ecology and epidemiology (Møller et al., 1998; Diggle et al., 2005; Rue et al., 2009; Simpson et al., 2011).

In this article,  $\mathcal{Y}$ , is second order stationary with minimally-parametrised covariance function,

$$\text{cov}[\mathcal{Y}(s_1), \mathcal{Y}(s_2)] = \sigma^2 r(\|s_2 - s_1\|/\phi), \quad (5)$$

where  $\sigma$  and  $\phi$  are known parameters. The parameter  $\sigma$  scales the log-intensity, whilst the parameter  $\phi$  governs the rate at which the correlation function decreases in space. The mean of the process  $\mathcal{Y}$  is set equal to  $-\sigma^2/2$  so as to give  $\mathbb{E}[\exp\{\mathcal{Y}\}] = 1$ .

Following Møller et al. (1998), Brix and Diggle (2001) and Diggle et al. (2005) we will use a discretised version,  $Y$ , of the above model, defined on a regular square grid. Strictly, observations  $X$  arising from the model are then cell counts on the grid, the intensity of the process being treated as constant within each cell. In practice, the aim is to make the lattice spacing sufficiently fine that cell-counts greater than 1 are rare and the error introduced by piece-wise constant approximation to the intensity is negligible.

Recall that the discretised  $Y$  is a finite collection of random variables, so the properties of  $\mathcal{Y}$  imply that  $Y$  has a multivariate Gaussian density with approximate covariance matrix  $\Sigma$ . The elements of  $\Sigma$  are calculated by evaluating Equation 5 at the centroids of the spatial grid

cells.

The next two sections present alternative methods for predictive inference of  $Y$  conditional on the observed data  $X$ .

## 4 Markov Chain Monte Carlo

The main advantage of the MCMC approach to inference for this model is that the ‘full covariance matrix’ of  $Y$  is used (compare with Section 5). Predictive inference about  $Y$  requires samples from the conditional distribution of the latent field,  $Y$ , given the observations,  $X$ , namely

$$\pi(Y|X) \propto \pi(X|Y)\pi(Y), \tag{6}$$

In order to evaluate  $\pi(Y)$  in Equation 6, the parameters of the process  $Y$  must either be known or estimated from the data. Estimation of  $\sigma$  and  $\phi$  can be achieved either in a Bayesian or likelihood-based framework, or by one of a number of more *ad hoc* methods e.g. Brix and Diggle (2001) and Diggle et al. (2005). These ad-hoc methods are described and implemented in the R package `lgcp`, see Taylor et al. (2011).

Markov chain Monte Carlo methods work by drawing a sequence of dependent samples from a target density of interest in situations where it is not possible to draw independent samples directly (e.g. via inversion of the cumulative distribution function). In the limit as the number of draws tends to infinity, the resulting output behaves as if it were a sample from the density of interest. In practice, if the chain appears to have converged to its stationary distribution and is mixing well, that is to say that the autocorrelation of the generated sample is low, then reliable inference can be made with relatively short runs. However, for non-trivial applications, the chain often mixes poorly, and it is difficult to tell whether stationarity has been achieved without prohibitively long runs to double-check that this is the case. Reviews of MCMC methodology include Gilks et al. (1995) and Gamerman and Lopes (2006).

The most well known MCMC method, the Metropolis Hastings (MH) algorithm (Metropolis et al., 1953; Hastings, 1970) is “arguably the most successful and influential Monte Carlo [technique]” (Girolami and Calderhead, 2011); along with Gibbs sampling, it is probably the most frequently employed method in the literature. Let  $\pi$  be the target density. Given a current state in the chain,  $Y$ , a new state,  $Y'$ , is proposed from any probability density,  $q(Y, Y') = \mathbb{P}(Y'|Y)$ , and accepted with probability,

$$\alpha(Y, Y') = \min \left\{ 1, \frac{\pi(Y'|X) q(Y', Y)}{\pi(Y|X) q(Y, Y')} \right\}. \quad (7)$$

A crucial step in designing an effective sampling regime is the choice of proposal kernel  $q$ . The word ‘choice’ both describes the specific probability density function associated with  $q$ , as well as any tuning parameters,  $h$ , that are associated with it. A very simple example is a random-walk kernel, where  $q(Y, Y') \sim \text{N}(Y, h^2)$ . For inference with the log-Gaussian Cox process, this article will focus on a more sophisticated, but well-studied version of the Metropolis-Hastings algorithm, the Metropolis-Adjusted Langevin algorithm.

Following Møller et al. (1998), Monte Carlo simulation from  $\pi(Y|X)$  is made more efficient by working with a linear transformation of  $Y^{\text{ext}}$ . Writing  $\Gamma = \Sigma_{\text{ext}}^{-1/2}(Y^{\text{ext}} - \sigma^2/2)$ , the target of interest is given by,

$$\pi(\Gamma|X) \propto \pi(X|Y^{\text{ext}})\pi(\Gamma), \quad (8)$$

When the gradient of the transition density can also be written down explicitly, a natural and efficient MCMC method for sampling from the predictive density of interest (Equation 8), is a Metropolis-Hastings algorithm with a Langevin-type proposal (Roberts and Tweedie, 1996; Møller et al., 1998),

$$q(\Gamma, \Gamma') = \text{N} \left[ \Gamma'; \Gamma + \frac{1}{2} \nabla \log \{ \pi(\Gamma|X) \}, h^2 \mathbb{I} \right],$$

where  $\text{N}(y; m, v)$  denotes a Gaussian density with mean  $m$  and variance  $v$  evaluated at  $y$ ,  $\mathbb{I}$  is the identity matrix and  $h > 0$  is a scaling parameter (Metropolis et al., 1953; Hastings,



1970).

Various theoretical results exist concerning the optimal acceptance probability of the MALA (Metropolis-Adjusted Langevin Algorithm); see Roberts and Rosenthal (1998) and Roberts and Rosenthal (2001). In practical applications, the target acceptance probability is often set to 0.574, which would be approximately optimal for a Gaussian target as the dimension of the problem tends to infinity. An algorithm for the automatic choice of  $h$  so that this acceptance probability is achieved without disturbing the ergodic property of the chain is detailed in Andrieu and Thoms (2008), and is implemented in the `lgcp` R package (Taylor et al., 2011).

In our case, the log of the target density (8) is given by

$$\log\{\pi(\gamma|X)\} = \text{constant} - \frac{1}{2}\|\gamma\|^2 + \sum_{s \in S} \{Y(s)X(s) - \mu C_A \lambda(s) \exp(Y(s))\},$$

where  $S$  is the set of grid cells in the observation window,  $C_A$  is the area of the individual grid cells and  $X(s)$  is the number of events in cell  $s$ . The gradient can be computed using the DFT,

$$\nabla \log\{\pi(\gamma|X)\}(s) = -\gamma(s) + \frac{1}{\text{length}\{\text{vec}[Y^{\text{ext}}]\}} \left( \text{DFT}\{E^{1/2} \odot \text{IDFT}[X - \mu C_A \lambda \exp(Y^{\text{ext}})]\} \right)(s),$$

where in this case,  $s$  is a cell in the extended grid.

## 5 The Integrated Nested Laplace Approximation

Further details on the material in this section are given in Rue et al. (2009). The Gaussian Markov random field/integrated nested Laplace approximation (GMRF/INLA) approach to inference for spatial log-Gaussian Cox processes relies on two different approximations. Firstly, an approximation to the full covariance matrix of  $Y$  is obtained, yielding substantial

computational benefits (see Section 2). Then, this approximate covariance takes the place of the full covariance in the model, and Bayesian inference is performed using the integrated nested Laplace approximation.

The integrated nested Laplace approximation delivers approximate inference for the posterior marginals of the latent field given the observed data and also for parameters of the latent field. Let  $\vartheta$  be hyperparameters of the latent field  $Y$ , noting that these are different to the parameters  $(\theta, \phi)$  mentioned above. INLA is based on standard results for marginal and conditional densities:

$$\begin{aligned}\pi(Y(s)|X) &= \int \pi(Y(s)|\vartheta, X)\pi(\vartheta|X)d\vartheta, \\ \pi(\vartheta_k|X) &= \int \pi(\vartheta|X)d\vartheta_{-k},\end{aligned}$$

Where, conditional on the observed data,  $\pi(Y(s)|X)$  is the posterior marginal density of the latent field at cell  $s$  and  $\pi(\vartheta_k|X)$  is the marginal posterior density of the  $k$ th component of  $\vartheta$ . With INLA, these exact relations are replaced by the approximations,

$$\begin{aligned}\tilde{\pi}(Y(s)|X) &= \int \tilde{\pi}(Y(s)|\vartheta, X)\tilde{\pi}(\vartheta|X)d\vartheta, \\ \tilde{\pi}(\vartheta_k|X) &= \int \tilde{\pi}(\vartheta|X)d\vartheta_{-k},\end{aligned}$$

where  $\tilde{\pi}$  denotes an approximation to a probability density function (pdf). The approximation of the joint density of the hyperparameters  $\vartheta$  uses

$$\tilde{\pi}(\vartheta|X) \propto \frac{\pi(Y, \vartheta, X)}{\pi_G(Y|\vartheta, X)} \Big|_{Y=Y^*(\vartheta)},$$

where  $\pi_G$  denotes a Gaussian approximation to a density and  $Y^*(\vartheta)$  is the mode of the full

conditional for  $Y$ . Lastly, the remaining undefined pdf is also approximated by a Gaussian,

$$\tilde{\pi}(Y(s)|\vartheta, X) = N[Y(s); \mu_s(\vartheta), \sigma_s^2(\vartheta)].$$

To evaluate the marginal posteriors, Rue et al. (2009) suggest a clever quadrature scheme over  $\vartheta$ . Optimised numerical routines for performing the above computations, and a large suite of other methods not covered in this article, are implemented in the R INLA package available from [www.r-inla.org](http://www.r-inla.org) (Rue et al., 2009).

For the simulation study below, Bayesian inference was performed using INLA’s `generic0` model. The default method for fitting this model includes a specification for the precision matrix,  $\tau Q_{\text{ext}}$ , where  $\tau$  is a hyperparameter with a log-gamma prior. For the application considered here, the parameter  $\tau$  is redundant because, having parametrised and estimated the precision matrix (as detailed in Section 2),  $\tilde{Q}_{\text{ext}}$  is a known quantity. The additional uncertainty induced by the default choice of prior was removed by fixing  $\tau = 1$ . Fixing  $\tau$  also considerably speeds up the time taken to fit the model. Since for the simulations, the mean  $\mu$  is known, the model was fitted without an offset (for those familiar with the INLA package, `form <- X~ -1 + f(...)`).

## 6 Simulation Results

### 6.1 The Simulated Scenarios

We simulated a total of 18 scenarios on a unit square observation window. We generated two different fixed spatial components,  $\lambda_1(s)$  and  $\lambda_2(s)$ , by scattering 200 points uniformly on the unit square and fitting a fixed-bandwidth bivariate Gaussian smoothing kernel to these, with respective standard deviations 0.04 and 0.1.

For each of the fixed spatial components, we used an exponential covariance model with all

combinations of  $\phi = 0.02, 0.04, 0.6$  and  $\sigma = 0.5, 1, 2$ . Since the latent field is exponentiated in the model, increasing values of  $\sigma$  make predictive inference more challenging for both MALA and INLA. We also hypothesised that larger values of  $\phi$  would present a greater challenge for the GMRF approximation step, and hence for the approximate inference step using INLA.

Note that for the full Gaussian field comparison below, we use the word 'INLA' to mean 'a GMRF approximation to the latent field followed by inference via the integrated nested Laplace approximation', this is distinct from the R library INLA.

Simulation and prediction took place on an identical grid size of  $128 \times 128$  in the extended space. This enabled a direct comparison of the true  $Y$  used to generate the data, and the predicted  $Y|X$  generated from the fitting processes. All computations were carried out on a 3.2GHz Intel(R) Core(TM) i5 desktop PC with 4Gb RAM.

## 6.2 Algorithm Parameters

For inference with MCMC, the sampler was set to run for 100,000 iterations with a 10,000 iteration burn-in and every 90th sample retained. The choice of 100,000 iterations was primarily for computational reasons: pilot runs had shown that results could be generated relatively quickly with this choice (in under 20 minutes), whilst the issue of convergence will be discussed in Section 6.3. The chain was initialised with  $\Gamma$  set to zero, corresponding to the mean of the field  $Y$ , i.e.  $-\sigma^2/2$ . For the adaptive MCMC, we used a method introduced by Andrieu and Thoms (2008) that is built into the `lgcp` package. This uses a Robbins-Munro stochastic approximation to adapt the tuning parameter of the proposal kernel (Robbins and Munro, 1951). At each iteration of the sampler, the tuning parameter is updated according to the iterative scheme,

$$h^{(i+1)} = h^{(i)} + \eta^{(i+1)}(\alpha^{(i)} - \alpha_{\text{opt}}),$$

where  $h(i)$  and  $\alpha^{(i)}$  are the tuning parameter and acceptance probability at iteration  $i$  and  $\alpha_{\text{opt}}$  is the target acceptance probability. The sequence  $\{\eta^{(i)}\}$  is chosen so that  $\sum_{i=0}^{\infty} \eta^{(i)}$  is infinite but for some  $\epsilon > 0$ ,  $\sum_{i=0}^{\infty} (\eta^{(i)})^{1+\epsilon}$  is finite. These two conditions ensure that any value of  $h$  can be reached, but in a way that maintains the ergodic behaviour of the chain. The class of sequences used in this simulation study was  $\eta^{(i)} = C/i^\alpha$  where  $\alpha = 0.5$  and  $C = 1$ ; the scheme was initialised with  $h = 1$  and set to target  $\alpha_{\text{opt}} = 0.574$ .

For inference with INLA, we compared a GMRF approximation using neighbourhood sizes of both 1 and 2. The first two methods employ a Gaussian approximation to the target (in INLA this corresponds to `strategy="simplified.laplace"`), which will henceforth be referred to as GAIN1 and GAIN2 ('GMRF Approximation followed by INLA'). The third method, GAIN3, employed a neighbourhood size of two and the full Laplace approximation to the target (`strategy="laplace"`). Fitting was achieved with INLA's `generic0` model, as discussed in Section 5.

### 6.3 Results

Mean computation times over the 18 scenarios are given in Table 2, these show that GAIN3 was the slowest, running in 39 minutes; MALA was next, running in 20 minutes; followed by GAIN2, in around 4 minutes; and GAIN1, which ran in around 1.5 minutes. These timings are based on the version of the INLA package as was available on 8<sup>th</sup> February 2012, we have since been informed by the authors that recent work on the `laplace` strategy could further reduce computation time by 30–50%.

	MALA	GAIN1	GAIN2	GAIN3
Mean Comp. Time (mins)	20.236	1.443	4.292	39.147
Variance	5.245	0.043	2.318	13.764

Table 2: Mean and variance of computation time for each algorithm.

Two measures were used to compare the performance of each method: the mean square error in estimating the latent field and a measure based on estimating probabilities. Details of the

Scenario	$\sigma$	$\phi$	MALA Last h	MSE			
				MALA	GAIN1	GAIN2	GAIN3
1	0.5	0.02	0.099	0.211	0.214	0.213	0.212
3	0.5	0.04	0.104	0.175	0.185	0.185	0.188
5	0.5	0.06	0.103	0.179	0.175	0.175	0.173
7	1	0.02	0.082	0.698	0.717	0.707	0.7
9	1	0.04	0.052	0.548	0.583	0.553	0.55
11	1	0.06	0.049	0.443	0.481	0.442	0.435
13	2	0.02	0.015	2.314	2.378	2.376	2.306
15	2	0.04	0.009	1.918	2.147	1.942	1.913
17	2	0.06	0.004	1.737	2.371	4.382	6.792
2	0.5	0.02	0.108	0.224	0.225	0.225	0.224
4	0.5	0.04	0.103	0.178	0.182	0.182	0.182
6	0.5	0.06	0.098	0.153	0.16	0.16	0.161
8	1	0.02	0.081	0.636	0.655	0.64	0.646
10	1	0.04	0.066	0.56	0.598	0.563	0.559
12	1	0.06	0.06	0.511	0.516	0.509	0.492
14	2	0.02	0.014	2.631	2.654	2.711	2.605
16	2	0.04	0.013	1.954	2.078	2.053	1.937
18	2	0.06	0.003	1.867	2.306	4.091	6.241

Table 3: Simulation results: dataset parameters, last value of  $h$  from MALA and mean square errors in predicting the true field. The upper half of the table gives results for fixed spatial  $\lambda_1(s)$ , the lower half results for fixed spatial  $\lambda_2(s)$ .

parameters for each scenario, the last value of  $h$  in the MALA run, and mean square errors are shown in Table 3. The mean square error was calculated as,

$$\text{MSE} = \frac{1}{M_{\text{in}}} \sum_s [Y(s) - \hat{Y}(s)]^2,$$

where  $M_{\text{in}}$  is the number of cells inside the observation window and the summation takes place over these cells. The results show that MALA gave marginally better point-wise prediction of the mean field. With the exception of scenarios 17 and 18, there is a tendency for INLA with a higher order neighbourhood structure to perform better, though the difference between the two implementations was only slight. These MSE's are presented to give the reader a sense of the increasing difficulty of the datasets. They cannot be used for comparing the algorithms because they contain no measure of estimated uncertainty in the latent field. In order to account for this uncertainty, we now introduce a measure of predictive ability. For each cell  $s$  inside the observation window, both MALA and INLA can produce a set of estimated quantiles, in this case for probabilities  $q_k \in q = \{0.01, 0.05, 0.1, 0.2, 0.3, 0.4, 0.5, 0.6, 0.7, 0.8, 0.9, 0.95, 0.99\}$ , that is a to say a set of thresholds,  $c_k(s)$ , satisfying,

$$\mathbb{P}[Y(s) \leq c_k(s)|X] = q_k.$$

Each algorithm yields a different set of estimated thresholds for each cell, say  $c^{(1)}(s) = \{c_k^{(1)}(s)\}$ ,  $c^{(2)}(s) = \{c_k^{(2)}(s)\}$  and  $c^{(3)}(s) = \{c_k^{(3)}(s)\}$  respectively for MALA, GAIN1 and GAIN2. Now, for  $l \in \{1, 2, 3\}$  we define

$$Z_k^{(l)}(s) = \mathbb{I}[Y(s) \leq c_k^{(l)}(s)],$$

where  $\mathbb{I}$  is the indicator function. Then,  $Z_k^{(l)}(s)$  is the indicator function of whether or not the true field in cell  $s$  was below the inferred threshold,  $c_k^{(l)}(s)$ , from method  $l$ . If  $c_k^{(l)}(s)$  is an

unbiased estimator of the true threshold,  $c_k^{\text{true}}(s)$ , then  $\mathbb{E}[Z_k^{(l)}(s)] = q_k$ , since,

$$q_k = \mathbb{P}[Y(s) \leq c_k^{\text{true}}(s)] = \mathbb{E} \left\{ \mathbb{P}[Y(s) \leq c_k^{(l)}(s) | X] \right\} = \mathbb{E} \left\{ \mathbb{E} \{ \mathbb{I}[Y(s) \leq c_k^{(l)}(s)] | X \} \right\} = \mathbb{E}[Z_k^{(l)}(s)].$$

The two measures of predictive ability are bias and mean squared error in estimating the probabilities,  $q_k$ , over the whole observation window. The ‘predictive mean square error’ was computed as,

$$\text{MSE}_2 = \frac{1}{13} \sum_{k=1}^{13} \left\{ \frac{1}{M_{\text{in}}} \sum_s [q_k - Z_k^{(l)}(s)]^2 \right\}.$$

The results are given in Table 4.

Scenario	GAIN1	GAIN2	GAIN3	Scenario	GAIN1	GAIN2	GAIN3
1*	2.697	2.258	1.594	2*	14.192	10.666	11.747
3*	2.801	2.748	3.553	4*	6.454	6.499	7.065
5	0.645	0.646	0.53	6*	3.149	3.15	3.719
7*	4.239	4.688	0.762	8*	4.077	1.49	6.719
9*	3.309	1.981	0.91	10*	2.449	1.34	0.471
11*	1.156	1.045	0.614	12	0.374	0.777	0.434
13*	26.929	82.41	0.531	14*	2.721	9.693	0.692
15*	84.014	60.145	0.558	16	0.457	3.62	1.131
17*	3.907	8.796	17.63	18*	36.912	135.375	311.099

Table 4: Mean square error in estimating probabilities,  $\text{MSE}_2$ , using each of the three INLA approximations, relative to  $\text{MSE}_2$  for the MALA algorithm. A \* in the first column indicates the scenarios where MALA outperformed GAIN1 and GAIN2. The left table are the results for fixed spatial  $\lambda_1(s)$  and the right table gives the values for fixed spatial  $\lambda_2(s)$ .

These results show that GAIN1 and GAIN2 outperformed MCMC in only two of the scenarios considered (5, 12 and 16). In the remaining scenarios, the relative mean squared error of GAIN2 varied from 1.045 to 82.41, the median being 3.38. Increasing the neighbourhood size from 1 to 2 did not lead to a median decrease in relative MSE, computed as the median of  $\text{MSE}_2(\text{GAIN2})/\text{MSE}_2(\text{GAIN1})$ . The median decrease in relative MSE comparing MALA to GAIN3 was 1 (the median of  $\text{MSE}_2(\text{GAIN3})/\text{MSE}_2(\text{MALA})$ ), although GAIN3 performed better in the scenarios with fixed spatial  $\lambda_1(s)$  compared with those with  $\lambda_2(s)$ , with respective values of 0.76 and 3.72.



The main source of these observed differences in predictive mean squared error is bias in the estimated probabilities. Figure 3 shows plots of estimated versus true probabilities in each of the 18 scenarios for each of the algorithms. The bias in these plots over the scenarios for both INLA algorithms is apparent in the ‘S’ shape around the line  $y = x$ , whereas for MCMC, the results are approximately symmetrically distributed about it. Additionally, these plots show that in two of the scenarios, both GAIN2 and GAIN3 would not give good estimates of probabilities.

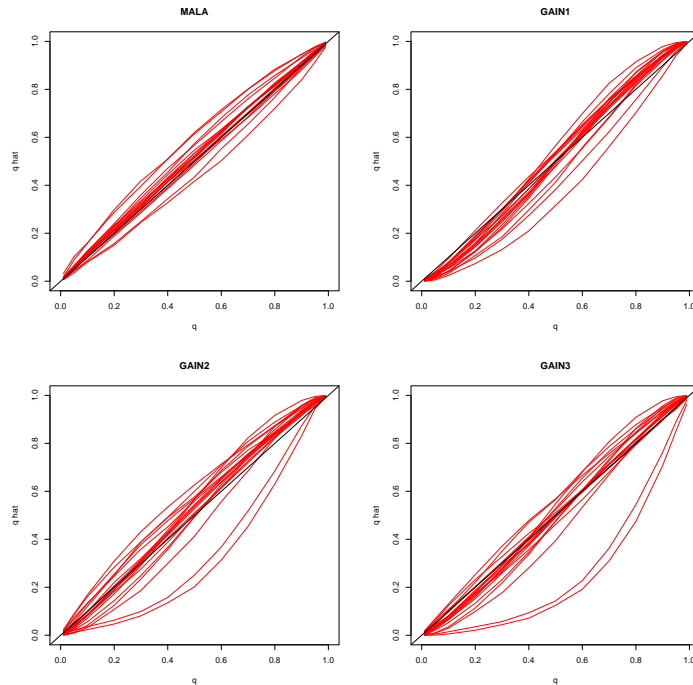


Figure 3: Illustrating the estimation of quantiles  $q_k$  by those inferred by each algorithm  $\hat{q}_k = \mathbb{E}[Z_k^{(l)}(s)]$  in scenarios 1–18. MALA in the top left plot, GAIN1 in the top right plot and GAIN2 in the bottom left plot and GAIN3 in the bottom right hand plot. For the MALA plot, the estimated quantiles are distributed about the line ‘ $y = x$ ’, whereas for the INLA-based methods, these fall in an ‘S’ shape around that line.

Our convergence diagnostics for MALA consisted of examining the cell-wise lag-1 autocorrelation of the MCMC chain. Example plots are shown in Figure 4; these were typical of the images produced in the blocks of scenarios 1–6, 7–12 and 13–18. The main feature of these plots is that in every case, the chain is mixing better (i.e. has lower lag-1 autocorrelation) in event-rich areas. Strictly, one should consider the mixing properties across all cells simulta-

neously, in which case the conclusion from this diagnostic would be that we would trust the results from scenarios 1–12, but worry about those from 13–18. However, due to a judicious choice of initial values for the chain (recall that  $\Gamma$  was initially set to zero), the effect of slow mixing in event-poor areas has less effect on the resulting inference than it might with a different set of initial values. Unconditionally,  $\mathbb{E}(Y) = -\sigma^2/2$ , so the chain in event-poor areas (sensibly) stays close to this value. In fact, a similar phenomenon occurs in INLA: in event-poor areas, the prediction surface tends to  $-\sigma^2/2$ . Despite the apparently slow mixing in scenarios 13–18, MALA still produces better predictive inference in each of these cases.

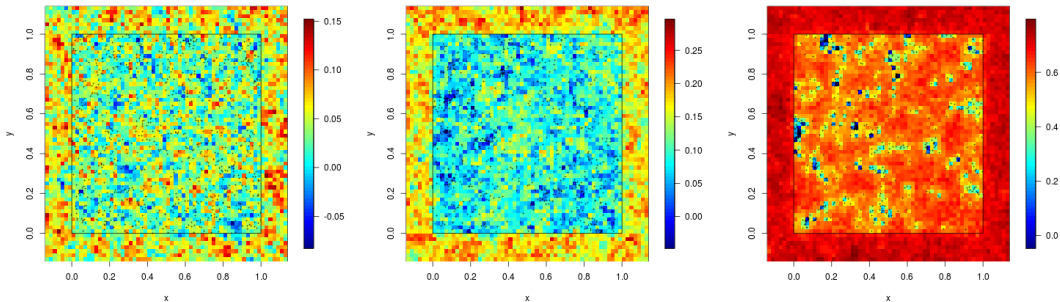


Figure 4: Image plots of lag-1 autocorrelation of the MCMC chain; the plots correspond to scenarios 4 (left), 10 (middle) and 16 (right). The plots for scenarios in respective blocks 1–6, 7–12 and 13–16 are similar in appearance. The box in the centre of the plot is the observation window and the data themselves appear as points on each plot.

To investigate whether the results for INLA were due to the approximation of the latent field, or whether they were due to error induced in the inference, we conducted a further simulation study. For each of the covariance functions defined by the parameter combinations in scenarios 1–18 above, we constructed a 2-neighbourhood GMRF approximation to the full covariance, and then simulated 18 further scenarios (1'–18') based on Gaussian variables simulated from the GMRF. In the following, INLA2 and INLA3 employ the same INLA settings as GAIN2 and GAIN3, but in this case there is no GMRF approximation step

Results from the second simulation study are shown in Table 6.3 and Figure 5. There are two main conclusions to be drawn from these results. Firstly, in Figure 5, the 'S' shape is no longer apparent for the INLA methods, however in the plot for INLA2, there is a noticeable

Scenario	INLA2	INLA3	Scenario	INLA2	INLA3
1'	0.207	0.8	2'*	1.922	0.913
3'*	8.146	0.637	4'*	3.381	0.933
5'	0.462	1.085	6'	0.344	1.141
7'*	6.506	0.726	8'*	15.142	0.622
9'*	1.773	1.759	10'*	55.562	1.743
11'^*	14.542	0.632	12'	0.032	1.365
13'^*	167.657	3.584	14'^*	40.266	6.144
15'^*	2.115	2.278	16'^*	56.126	2.5
17'^*	2.708	0.874	18'	0.545	2.586

Mean square error in estimating probabilities,  $MSE_2$ , using each of the three INLA approximations, relative to  $MSE_2$  for the MALA algorithm. A \* in the first column indicates the scenarios where MALA outperformed INLA2. The left table are the results for fixed spatial  $\lambda_1(s)$  and the right table gives the values for fixed spatial  $\lambda_2(s)$ .

upward bias in the centre of the plot. Also from the plots, it is clear that MALA did not perform well on two occasions, and INLA on one. The main second conclusion from this simulation study is despite the fact that INLA now shows less bias, MALA nevertheless still outperforms both INLA2 and INLA3. The median relative increase in MSE comparing MALA to INLA2 was 3 over all scenarios and 1.1 comparing MALA to INLA3. As was the case for scenarios 1–18, MALA performs better for fixed spatial  $\lambda_2(s)$ , with a median increase of 1.37 for INLA3 whereas for  $\lambda_1(s)$ , INLA3 performed better at a median increase of 0.87.

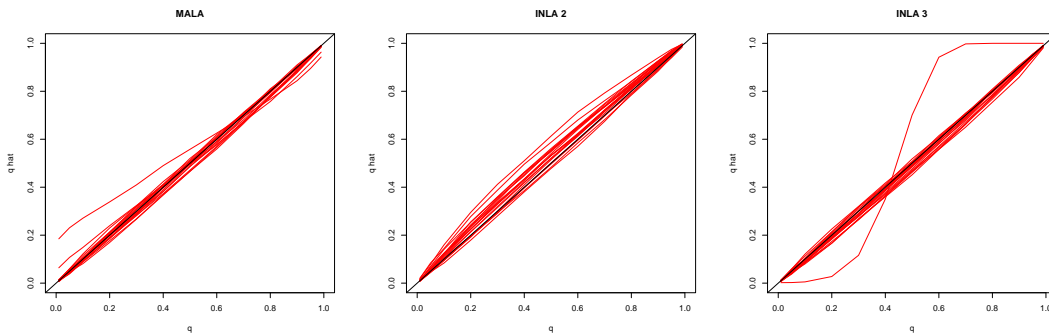


Figure 5: Illustrating the estimation of quantiles  $q_k$  by those inferred by each algorithm  $\hat{q}_k = \mathbb{E}[Z_k^{(l)}(s)]$  in scenarios 1'–18'. MALA in left plot, GAIN2 in the middle plot and GAIN3 in the right hand plot.

## 7 Discussion

In this article, we have provided a tour of the mathematical and statistical techniques behind spatial prediction for log-Gaussian Cox processes. We have independently evaluated a previously published method for approximating spatially continuous Gaussian processes with GMRF and conducted a critical comparison of two methodologies for predictive Bayesian inference in this class of models.

A suite of functions (as well as wrapper functions for the approximate Bayesian predictive inference for INLA) have been made freely available in the `lgcp` R package (Taylor et al., 2011). Our restriction in this paper to spatial, rather than spatio-temporal prediction is primarily ease of exposition. However, and unsurprisingly, the spatio-temporal concept is computationally more demanding. In pilot runs, even INLA was found to be quite slow for spatio-temporal prediction on a regular grid, due to the hugely increased dimensionality of the problem and a corresponding increase in the complexity of dependence patterns in the precision matrix (see Section 2). Furthermore, we have restricted our choice of MCMC methods to the Metropolis adjusted Langevin algorithm (MALA) rather than investigating more sophisticated sampling techniques such as Riemann manifold Langevin or Hamiltonian Monte Carlo (Girolami and Calderhead, 2011). Our reasons for this choice are ease of implementation, stability and the fact that MALA has been well studied in the literature, with various theoretical results available concerning practical implementation. The authors are aware that the methods of Girolami and Calderhead (2011) have better theoretical mixing properties.

We have demonstrated that MCMC can yield more accurate estimates of predictive probabilities compared with INLA-based methods for this class of models, depending on the chosen settings. Furthermore the predictive probabilities from MCMC can be obtained comparatively quickly, and show less bias compared with those from INLA. The inferential technique of producing a GMRF approximation to a Gaussian field and then performing inference via

the integrated nested Laplace approximation should therefore be regarded with appropriate caution. This article also opens up the question of the utility of gradient-based MCMC methods for inference in log-Gaussian Cox process models assuming a latent Gaussian Markov random field; the default method of inference for these models would appear to be a blocked Gibbs sampling strategy eg. Rue et al. (2009).

We have not addressed the full capabilities of both software implementations: `lgcp` and `INLA`. In particular, `INLA` provides access to inference for a wide class of latent Gaussian models, whilst `lgcp` is restricted to spatial and spatio-temporal log-Gaussian Cox processes. Furthermore, the `INLA` package also provides a framework for the estimation of hyperparameters, which `lgcp` does not; this is known to be a very challenging sampling task for MCMC.

## References

- Andrieu, C. and J. Thoms (2008). A tutorial on adaptive MCMC. *Statistics and Computing* 18(4), 343–373.
- Brix, A. and P. J. Diggle (2001). Spatiotemporal prediction for log-gaussian cox processes. *Journal of the Royal Statistical Society, Series B* 63(4), 823–841.
- Diggle, P., B. Rowlingson, and T. Su (2005). Point process methodology for on-line spatio-temporal disease surveillance. *Environmetrics* 16(5), 423–434.
- Frigo, M. and S. G. Johnson (2011). FFTW fastest Fourier transform in the west. <http://www.fftw.org/>.
- Gamerman, D. and H. F. Lopes (2006). Markov chain Monte Carlo: Stochastic simulation for Bayesian inference (2nd ed.).
- Gelfand, A., P. Diggle, M. Fuentes, and P. Guttorp (Eds.) (2010). *Handbook of Spatial Statistics*. Chapman and Hall.

- Gilks, W., S. Richardson, and D. Spiegelhalter (Eds.) (1995). *Markov Chain Monte Carlo in Practice*. Chapman & Hall/CRC.
- Girolami, M. and B. Calderhead (2011). Riemann manifold Langevin and Hamiltonian Monte Carlo methods. *Journal of the Royal Statistical Society, Series B* 73(2), 123–214.
- Hastings, W. K. (1970). Monte Carlo sampling methods using Markov chains and their applications. *Biometrika* 57(1), 97–109.
- Krey, S., U. Ligges, and O. Mersmanne (2011). R package fftw. <http://cran.r-project.org/web/packages/fftw/index.html>.
- Lindgren, F., H. Rue, and J. Lindström (2011). An explicit link between gaussian fields and gaussian markov random fields: the stochastic partial differential equation approach. *Journal of the Royal Statistical Society, Series B* 73(4), 423–498.
- Metropolis, N., A. W. Rosenbluth, M. N. Rosenbluth, A. H. Teller, and E. Teller (1953). Equation of state calculations by fast computing machines. *The Journal of Chemical Physics* 21(6), 1087–1092.
- Møller, J., A. R. Syversveen, and R. P. Waagepetersen (1998). Log Gaussian Cox processes. *Scandinavian Journal of Statistics* 25(3), 451–482.
- Robbins, H. and S. Munro (1951). A stochastic approximation methods. *The Annals of Mathematical Statistics* 22(3), 400–407.
- Roberts, G. and J. Rosenthal (2001). Optimal scaling for various Metropolis-Hastings algorithms. *Statistical Science* 16(4), 351–367.
- Roberts, G. O. and J. S. Rosenthal (1998). Optimal scaling of discrete approximations to langevin diffusions. *Journal of the Royal Statistical Society: Series B (Statistical Methodology)* 60, 255–268(14).
- Roberts, G. O. and R. L. Tweedie (1996). Exponential convergence of Langevin distributions and their discrete approximations. *Bernoulli* 2(4), pp. 341–363.

- Rue, H. and L. Held (2005). *Gaussian Markov Random Fields*. Chapman & Hall.
- Rue, H., S. Martino, and N. Chopin (2009). Approximate bayesian inference for latent gaussian models by using integrated nested laplace approximations. *Journal of the Royal Statistical Society, Series B* 71(2), 319–392.
- Simpson, D., J. Illian, F. Lindgren, S. H. Sørbye, and H. Rue (2011). Going off grid: Computationally efficient inference for log-Gaussian Cox processes. Preprint in Statistics No. 10/2011, NTNU.
- Taylor, B., T. Davies, B. Rowlingson, and P. Diggle (2011). lgcp – an R package for inference with spatiotemporal log-Gaussian Cox processes. Submitted, available from url-  
<http://www.arxiv.org/pdf/1110.6054>.
- Wood, A. T. A. and G. Chan (1994). Simulation of stationary gaussian processes in  $[0,1]^d$ . *Journal of Computational and Graphical Statistics* 3(4), 409–432.